SENSING CAPABILITIES AND GAUGE FACTOR OF A MULTISCALE MULTIPHASE GRAPHENE-BASED COMPOSITE

N. Hostettler[1,2], P. Hubert[1,2*]
[1] Structures and Composite Materials Laboratory, McGill University, Montréal, Canada
[2] Centre de recherche sur les systèmes polymères et composites à haute performance (CREPEC)
* Corresponding author (pascal.hubert@mcgill.ca)

Keywords: *Self-sensing, multiscale composite, health monitoring*

ABSTRACT

The brittle nature of composite material makes them prone to failure, leading to high repair and maintenance costs. By adding graphene to a multiphase resin system, it is possible to create a self-assembly network of graphene leading to self-sensing properties from a measure of resistivity. For such material to be adopted into real applications, a characterization of its sensing capabilities is needed in several different loading mode to study its behaviour. This was done by reinforcing the resin system with a fibreglass preform and testing it in traction, 3- and 4-point bending. The resistivity change was recorded during each of these tests to assess its relation to stress and strain, and to calculate its gauge factor. In each case, the evolution of resistivity was found linearly linked with the applied stress and strain. That allowed to have a direct calculation of the elastic modulus from the resistivity and either the stress or strain. The gauge factors were found different between traction and bending. This was shown to be an effect of the traction/compression load superposition in bending. The reliable changes obtained in resistivity with strain and stress together with high gauge factor makes this material a strong candidate for future self-sensing application.

1 INTRODUCTION

The addition of graphene to fibre reinforced plastics (FRPs) has many well-known advantages, one being the increase of toughness and electrical conductivity [1]. This improvement in electrical properties unlock interesting applications for such system as actuators, fuel cells, photodetectors or mechanical sensors [2]. The latter is of interest since it allows direct tracking of the deformation and damage during a part's life by simply probing its resistivity, optimizing the part maintenance and repair [3]. Several studies were published in this scope [4] [5] [6]; however, it usually uses high purity chemical vapor deposition (CVD) graphene or carbon nanotubes (CNTs) that are expensive and comes at low production volumes. The alternative few-layers graphene (FLG) is required in larger amount to reach the conductivity threshold, decreasing the processability of the part. It is possible to create a self-assembly continuous network of graphene particles by blending the thermoset resin with a thermoplastic which shifts and lower the percolation threshold [1]. This reduces the quantity of FLG needed for conduction and increases the toughness of the system. It is then possible to produce cost-effective self-sensing composite parts. When other researches have shown the efficiency of such system, it was mostly on non-reinforced systems, either in traction or compression. This paper focuses on the study of the electrical response of such systems to different loading modes (traction, 3 and 4-point bending), its link to the elastic modulus, and the sensing sensibility of the system measuring its gauge factor.

2 MATERIALS & METHODS

2.1 Materials

The resin system was composed on a blend of Polylite 31289 from *Reichhold*, a pre-accelerated unsaturated polyester (UP) and 2 wt% of CAPA6500, a polycaprolactone (PCL) from *Ingevity*. This system was cured with 2 wt% of Norox Azox from *United-initiator*. To this was incorporated 6 wt% of GrapheneBlack3X from *NanoXplore*, an industrial grade few-layer graphene (FLG) with a primary particle size between 1-2 µm and an agglomerate size of $D50 = 38\ \mu m$, 6 to 10 graphene layers in thickness and a carbon to oxygen ratio of 96:1 [7]. This specific blend composition leads to a phase separated morphology with a preferential localisation of the graphene particles in the UP-rich region. This configuration strongly enhances the toughness of the system and reduces its percolation threshold [1]. The dispersion of the graphene was optimized by incorporating 1 wt% of Triton X100 diluted 15:1 in styrene as a surfactant, both from *SigmaAldrich*. Finally, the resin system was reinforced with a bidirectional-E glass-complex 0/90/Mat preform with a superficial density of 910 g/m^2 from *SAERTEX*.

2.2 Methods

2.2.1 Processing

The unsaturated polyester resin was weighted into a glass jar, the correct mount of graphene was added together with the surfactant and dispersed with a probe sonicator (*Hielscher* UP400St) for two cycles of 7 min spaced by a 15 min cool down step to limit the temperature increase below 70°C. The jar was then transferred into a 65°C water bath where the PCL was added and was mechanically stirred for 20 min until homogeneous. The system was then let to rest at room temperature for 20 min to cool down and stabilize the phase-separated morphology. Next, the initiator was incorporated, and the system was degassed for a 1-2 minutes to be ready for processing. The processing was conducted by compression resin transfer moulding on an MTS 250 kN servo-hydraulic testing machine with a 100 x 100 mm picture frame mould. The surface of the mould was prepared with Chemlease 2752W from *ChemTrend* to ease demoulding. The fibreglass preform $[Mat/90/0]_s$ was set into the mould topped with a 3.8 mm thick metallic shim frame (outer and inner size of 100 and 80 mm respectively) to create a pinching zone and favour the impregnation of the fibre tows. The plates were pressed to a target thickness of 1.8 mm (V_f = 0.4) at 0.05 mm/s and let to rest (mould closed to help impregnation of the fibre) for 7 min before increasing the temperature to 50°C for an additional 7 min to cure the resin. The plates were demoulded and post-cured in an oven at 120°C for 2 h to complete the cure.

2.2.2 Mechanical tests and sensing capabilities

The sensing capabilities were investigated with three different loading modes: (i) 3-point bending, (ii) 4-point bending and (iii) traction. They were conducted on 20 x 70 mm coupons (0° fibres at the neutral axis) on an MTS 5 kN universal testing machine at room temperature. Each test consisted of 5 load/unload at different load amplitude and separated by a 15 s waiting period; the first cycle was discarded from the analysis as it is usually highly asymmetric. The span for the 3- and 4-point bending were selected according to the ASTM D7264. The traction tests were conducted according to ASTM D3039, the displacement was probed with an MTS extensometer. To reduce the influence of the grips and to electrically isolate the sample from the testing machine, 10 x 20 mm composite tabs (UP Neat and fibreglass) were glued on each side and at each end of the traction sample. For the bending tests, 3 mm wide silver paint electrode (*SPI-supplies)* were painted on each end of the sample. Similar electrodes were painted on the traction sample but after the tabs leaving a ~ 30 mm distance between each electrode. The resistivity was probed during the mechanical tests with a *Keithley* 6517A with a 10 V voltage directly applied on the silver electrodes. The resistivity was then calculated as:

$$\rho = \frac{RA}{l} = \frac{1}{\sigma} \qquad (1)$$

where $A = t \cdot w$ is the cross section of the sample, R the measured resistance, l the distance in-between the electrodes and σ the conductivity. The sensibility of the sensing capabilities was measured with the gauge factor calculated as:

$$GF = \frac{\Delta R}{R_0 \epsilon} \qquad (2)$$

where $\Delta R = R - R_0$ is the instantaneous change in resistivity, R_0 is the initial resistance and ϵ is the applied strain measured from the displacement data. Two types of tests were conducted: (i) an amplitude study where the shape of the resistivity response was studied depending on the loading mode and load amplitude at a constant testing rate of 0.1 mm/s, and (ii) a strain rate study in traction, where the sample was loaded to 0.5 kN at different strain rate to assess the impact of the testing speed on the gauge factor.

3 RESULTS & DISCUSSION

3.1 Sensing capabilities

The evolution of the resistance during cycling is shown for each loading mode in Figure 1. The electric response is strong and consistent between each cycle confirming a deformation in the elastic region. As a plastic deformation would be characterized by a reduction of the number of electron paths leading to an increase of the baseline towards higher resistance. Two different behaviours are observed, both 3- and 4-point bending resulted in a decrease in the overall resistance of the system while the traction resulted in an increase in resistance. This is explained by the type of stress distribution in each loading mode. In traction the graphene particles are pulled away from each other breaking direct electron paths and increasing the tunneling distance which resulted in an overall increase of the resistance [4] [8] (see Figure 1.c). For the bending case, literature predicts a behaviour similar to traction with an increase in resistivity [9] [10], the tests were, however, performed on non-reinforced system. The presence of fibres strongly effects the resistivity vs. strain behaviour and leads to a decrease in resistivity (see Figure 1.a and b). In bending, the stress is composed on a coupling of traction (bottom half of the sample) and compression (upper half of the sample). A decrease in resistance is a sign that the graphene particles were pushed closer to each other, creating new conducting paths and lowering the tunneling distance [4] [11]. In the regime tested here, the deformation was then dominated by the compression of the upper surface of the sample. This can be shown calculating the strain in the upper and lower part of the sample: under the assumption that the upper and bottom half part of the sample have a homogeneous compression and traction modulus E_C and E_T, respectively (measured on the traction sample). From the force equilibrium of the system, the position of the neutral axes from the bottom of the sample h_b can be calculated as:

$$h_b = \frac{h}{1 + \left(\frac{E_t}{E_c}\right)^{1/2}} \cong 0.86\, mm \qquad (3)$$

with $h = 1.8\, mm$ the thickness of the sample. Due to the different behaviour of the sample in traction and compression, the neutral axis is slightly shifted downward, the bottom half of the sample being stiffer than the upper part. From this the strain at the top and bottom of the sample can be calculated as:

$$\epsilon_t = \frac{FLE_C(h - h_b)}{4D} \qquad (4)$$

$$\epsilon_b = \frac{FLE_T h_b}{4D} \qquad (5)$$

Where F is the applied force, L the span length and D the flexural stiffness defined as:

$$D = \frac{h}{3}\left(h_b^3 E_t + (h - h_b)^3 E_c\right) \qquad (6)$$

Doing so, we find a compression strain ~ 7.44% larger with 3- and 4-point bending, following a similar approach, both independent from the applied load. This difference explains the dominant reduction of resistivity in the bending loading modes. A characteristic second upward peak is, however, observed during each cycle in both 3- and 4-points bending, sign that the traction compression superposition is also present in the resistivity data.

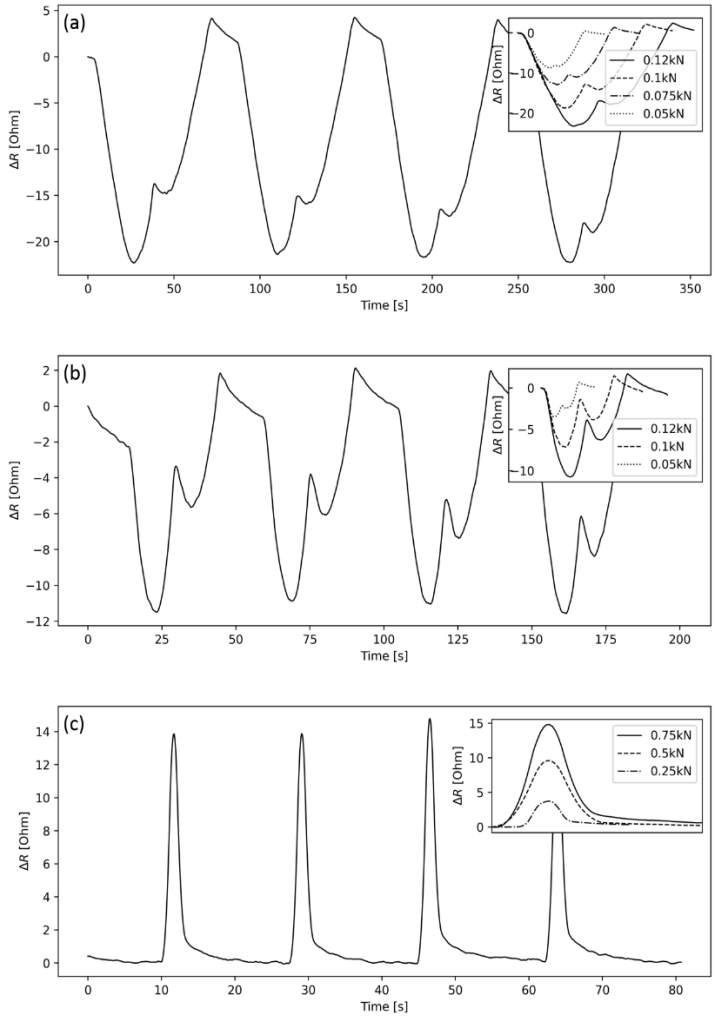

Figure 1: Resistance evolution with a 0.75 kN applied load and different load amplitudes (top right inserts) for: (a) 3-point bending, (b) 4-point bending and (c) traction.

The evolution of the resistivity with the applied force and applied strain is shown in Figure 2. Note that for readability, the absolute values of the data are depicted. The behaviour for each loading mode follows a close linear trend. The relation of the resistivity is similar between the force and strain, sign that a measure of resistivity could be used to indirectly measure either the force or strain, or the elastic modulus. This is shown in the following equations:

$$\begin{aligned} \sigma(\Delta\rho) &= n_{\Delta\rho}\Delta\rho, \\ \Delta\rho(\epsilon) &= n_\epsilon \epsilon \\ \Rightarrow \sigma(\epsilon) &= n_{\Delta\rho} n_\epsilon \epsilon \stackrel{?}{=} E_y \epsilon \end{aligned} \qquad (7)$$

where σ is the stress, $n_{\Delta\rho}$ the slope of the stress vs. resistivity curve, n_ϵ the slope of the resistivity vs. strain curve and E_y the slope of the stress vs. strain curve (the elastic modulus).

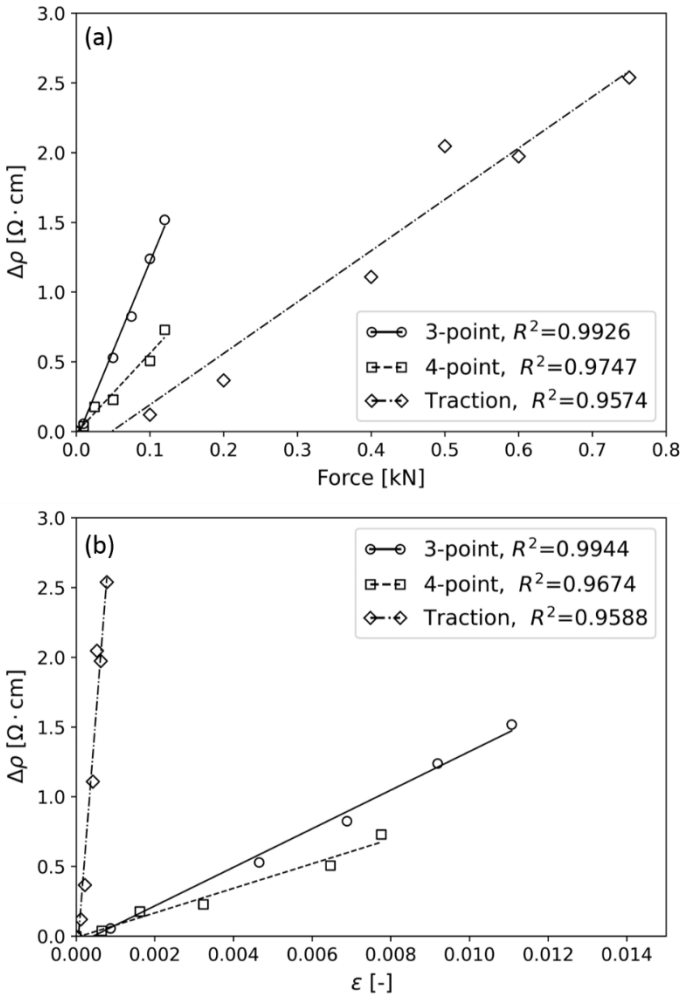

Figure 2: Resistivity evolution with (a) applied load and (b) applied strain.

The resulting modulus calculated from the resistivity data, $n_{\Delta\rho}\mathrm{n}_\epsilon$, and from the usual stress vs. strain data, E_y, are compared in Table 1. Both methods lead to similar values of modulus confirming the possibility to use such materials as a reliable intrinsic stress or strain sensor.

Table 1: Comparison between the elastic modulus calculated from the resistivity and from the strain data.

	$n_{\Delta\rho} \cdot \mathrm{n}_\epsilon$ $[GPa]$	E_y $[GPa]$
3-point	4.4321	4.4327
4-point	4.3092	4.3091
traction	26.255	27.402

3.2 Gauge factor

The average gauge factor from each load amplitude and strain rate were calculated from Equation 2 and are displayed in Table 2. The gauge factor measured in traction appear larger than the one in 3- and 4-point bending. This is explained by the dual traction/compression observed in flexion. Assuming the effect on the resistivity to be similar in traction and compression, in 3-point only 7% of the strain is contributing to the "apparent" gauge factor. The real gauge factor in compression can then be estimated by scaling the apparent gauge factor to 100% as follow:

$$GF_c = \frac{GF_a}{\left(1 - \frac{\epsilon_t}{\epsilon_c}\right)} \qquad (8)$$

Doing so, it gives $GF_c = 16.16$ for 3-points and $GF_c = 11.14$ for 4-point bending, which is close to the actual compression gauge factor of the system. The proposed assumption on competing creation/destruction of electron paths is then validated. Note that these gauge factors are on the order of what is found in literature [4].

Table 2: Average gauge factor over the whole force range for the three-loading mode.

	GF
3-point	1.12 ± 0.29
4-point	0.83 ± 0.19
traction	22.19 ± 6.28
compression	17.31 ± 4.65

3.3 Gauge factor vs. strain rate

The strain rate influence on the gauge factor is vital in determining the suitability of using such material in real conditions. The evolution of the gauge factor as a function of the strain rate on the traction sample is shown in Figure 3. Both traction and compression where performed. In both cases, the gauge factor is linearly decreasing as the strain rate is increased. This is a viscoelastic effect reducing the strain at higher test speed, which in its turn reduces the measured change in resistivity. The difference in slopes between the two cases is again due to the different behaviour of the material in traction and compression.

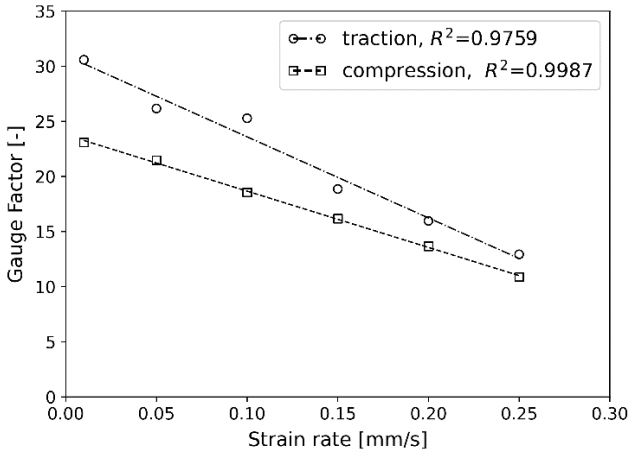

Figure 3: Evolution of the gauge factor as a function of the strain rate for the traction sample both in traction and compression.

4 CONCLUSIONS

The sensing capabilities of multiscale multiphase graphene-based composites was studied for three loading mode: traction, 3-point and 4-point bending. For each of them the shape as well as the influence of the load amplitude was studied. A clear link between the shape and the strain distribution through the sample thickness was found, exposing the coupled loading mode of bending (traction/compression). This observation was found to also apply to the gauge factor where the gauge factor in traction was retrieved from the bending tests. It was also demonstrated that such material can be used as strain/stress sensor, and successfully estimate the elastic modulus from the resistivity data. An increased strain rate was found to reduce the measured gauge factor due to the viscoelasticity nature of the system. However, this material system can be reliably used either as a strain sensor or as a force sensor in the elastic region with all three loading modes, or a coupling of them.

ACKNOWLEDGEMENTS

The authors thank their partners, Dr. Giovanna Gutiérrez and Dr. Abdou Khadri Diallo from NanoXplore Inc. for their helpful insights and feedback, NanoXplore Inc. for donating the graphene and the polyester resin, Ingevity for donating the thermoplastic, the Natural Sciences and Engineering Research Council of Canada (NSERC), Prima Quebec, the Research Center for High Performance Polymer and Composite Systems (CREPEC).

REFERENCES

[1] N. Hostettler et P. Hubert, «A phase separation strategy for enhanced toughness self-assembly graphene-network composites,» *Composites Science and Technology*, vol. 225, p. 109503, 2022.

[2] R. Taherian et A. Kausar, Electrical Conductivity in Polymer-Based Composites, William Andrew, 2019.

[3] H. Liu, Y. Li, K. Dai, G. Zheng, C. Liu, C. Shen, X. Yan, J. Guo et Z. Guo, «Electrically conductive elastomer nanocomposites at ultralow graphene loading levels for strain sensor applications,» *Journal of Materials Chemistry C*, vol. 4, pp. 157-166, 2015.

[4] A. J. Marsden, D. G. Papageorgiou, C. Vallés, A. Liscio, V. Palermo, M. A. Bissett, R. J. Young et I. A. Kinloch, «Electrical percolation in graphene-polymer composites,» *2D Materials*, vol. 5, n° %13, 2018.

[5] C. Buggisch, A. Gagani et B. Fiedler, «Capacitance measurements on integrated conductors for detection of matrix cracks in GFRP,» *Functional Composite Materials*, vol. 2, pp. 1-13, 2021.

[6] C. Buggisch, D. Gibhardt, N. Felmet, Y. Tetzner et B. Fiedler, «Strain sensing in GFRP via fully integrated carbon nanotube epoxy film sensors,» *Composites Part C: Open Access*, vol. 6, p. 100191, 2021.

[7] NanoXplore Inc, «Technical Data Sheet - GrapheneBlack3X DS-GB 3X-21080, Technical Report,» 2021.

[8] S. Han, Q. Meng, A. Chand, S. Wang, X. Li, H. Kang et T. Liu, «A comparative study of two graphene based elastomeric composite sensors,» *Polymer Testing*, vol. 80, p. 106106, 2019.

[9] A. Tamburrano, F. Sarasini, G. De Bellis, A. G. D'Aloia et M. S. Sarto, «The piezoresistive effect in graphene-based polymeric composites,» *Nanotechnology*, vol. 24, p. 465702, 2013.

[10] P. Costa, J. Nunes-Pereira, J. Oliveira, J. Silva, J. Agostinho Moreira, S. Carabineiro, J. Buijnsters et S. Lanceros-Mendez, «High-performance graphene-based carbon nanofiller/polymer composites for piezoresistive sensor applications,» *Composites Science and Technology*, vol. 153, pp. 241-252, 2017.

[11] H. Yang, L. Yuan, X. Yao et D. Fang, «Piezoresistive response of graphene rubber composites considering considering the tunneling effect,» *Journal of the Mechanics and Physics of Solids*, vol. 139, p. 103943, 2020.